7-2011

Advances in developing multiscale flaw models for eddy-current NDE

R. Kim Murphy
Victor Technologies, LLC

Harold A. Sabbagh
Victor Technologies, LLC

John R. Bowler
Iowa State University, jbowler@iastate.edu

Yuan Ji
Iowa State University

Elias H. Sabbagh
Victor Technologies, LLC

See next page for additional authors

Advances in developing multiscale flaw models for eddy-current NDE

R. Kim Murphy, Harold A. Sabbagh, John R. Bowler, Yuan Ji, Elias H. Sabbagh et al.

Citation: AIP Conf. Proc. **1430**, 309 (2012); doi: 10.1063/1.4716244
View online: http://dx.doi.org/10.1063/1.4716244
View Table of Contents: http://proceedings.aip.org/dbt/dbt.jsp?KEY=APCPCS&Volume=1430&Issue=1
Published by the American Institute of Physics.

ADVANCES IN DEVELOPING MULTISCALE FLAW MODELS FOR EDDY-CURRENT NDE

R. Kim Murphy[1], Harold A. Sabbagh[1], John R. Bowler[3], Yuan Ji[3], Elias H. Sabbagh[1] and John C. Aldrin[2]

[1] Victor Technologies, LLC, Bloomington, IN
[2] Computational Tools, Gurnee, IL
[3] Iowa State University, Ames, IA

ABSTRACT. The need to accurately model multiscale phenomena is ubiquitous in eddy-current nondestructive evaluation. By using volume-integral equations, we are able to develop a very simple algorithm for accurately computing the response of a very small anomaly in the presence of a much larger one. We validate the algorithm and its associated code in **VIC-3D©** through benchmark data on two test sets: (1) a notch at a bolt hole with an upper surface coil, and (2) a notch in a bolt hole with a plate surface coil.

Keywords: Eddy-Current Nondestructive Evaluation, Volume-Integral Equations, Electromagnetic Forward and Inverse Problems, Multiscale Phenomena
PACS: 02.50.-r, 81.70.-q

INTRODUCTION

The use of integral equations and anomalous currents allows us to efficiently remove 'background effects' in either forward or inverse modeling. Consider the anomalous region within a background host, as shown in Figure 1. Let $\sigma_b(\mathbf{r})$ be the conductivity when the flaw is absent. Outside the background region, $\sigma_b(\mathbf{r})$ is equal to the host conductivity, σ_h. Inside the background regions it varies with position, $\mathbf{r}$. Let $\sigma(\mathbf{r})$ be the conductivity when the flaw is present. Outside the background region, $\sigma(\mathbf{r})$ is equal to the host conductivity. Inside the background region, but outside the flaw, $\sigma(\mathbf{r}) = \sigma_b(\mathbf{r})$. Inside the flaw, $\sigma(\mathbf{r})$ is not equal to $\sigma_b(\mathbf{r})$, but varies with position.

First, consider the unflawed background region. The anomalous current for this problem satisfies

$$\mathbf{J}_b(\mathbf{r}) = (\sigma_b(\mathbf{r}) - \sigma_h)(\mathbf{E}_{in}(\mathbf{r}) + \mathbf{E}(\mathbf{r})[\mathbf{J}_b]) \ , \tag{1}$$

where the functional notation, $\mathbf{E}(\mathbf{r})[\mathbf{J}_b]$, implies an integral operator on $\mathbf{J}_b$, whose kernel is a Green's function [1].

Next, consider the flawed background region, and define anomalous currents

$$\begin{aligned} \mathbf{J}_f(\mathbf{r}) &= (\sigma(\mathbf{r}) - \sigma_b(\mathbf{r}))(\mathbf{E}_{in}(\mathbf{r}) + \mathbf{E}(\mathbf{r})[\mathbf{J}_f]) & (2) \\ \mathbf{J}_d(\mathbf{r}) &= (\sigma_b(\mathbf{r}) - \sigma_h)(\mathbf{E}_{in}(\mathbf{r}) + \mathbf{E}(\mathbf{r})[\mathbf{J}_f] + \mathbf{E}(\mathbf{r})[\mathbf{J}_d]) \\ &+ (\sigma(\mathbf{r}) - \sigma_b(\mathbf{r}))\mathbf{E}(\mathbf{r})[\mathbf{J}_d] \ . & (3) \end{aligned}$$

Review of Progress in Quantitative Nondestructive Evaluation
AIP Conf. Proc. 1430, 309-315 (2012); doi: 10.1063/1.4716244

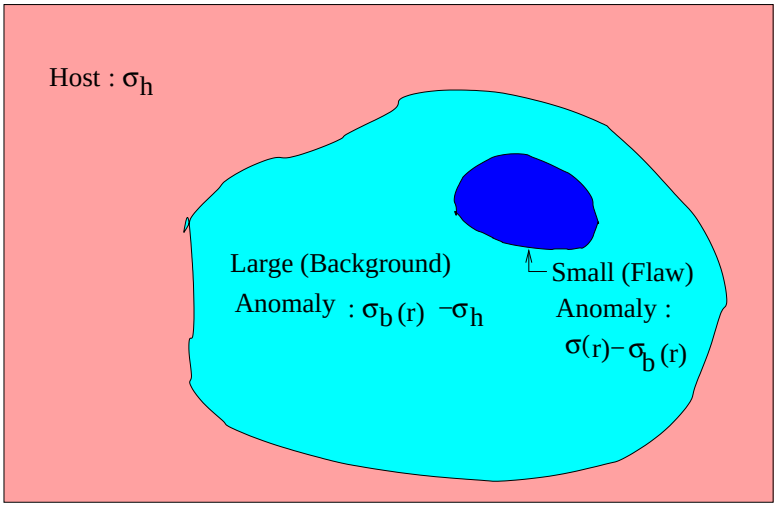

FIGURE 1. Defining an anomalous region within a background host. $\sigma_b(\mathbf{r}) - \sigma_h$ is the anomalous conductivity associated with the 'large' background, and $\sigma(\mathbf{r}) - \sigma_b(\mathbf{r})$ is the anomalous conductivity associated with the 'small' flaw.

The anomalous current, $\mathbf{J}_a = \mathbf{J}_d + \mathbf{J}_f$, satisfies $\mathbf{J}_a = (\sigma(\mathbf{r}) - \sigma_h)(\mathbf{E}_{in} + \mathbf{E}(\mathbf{r})[\mathbf{J}_f] + \mathbf{E}(\mathbf{r})[\mathbf{J}_d])$.

The change in impedance due to the flaw is

$$\begin{aligned} \mathbf{E}_{in} \cdot \mathbf{J}_a - \mathbf{E}_{in} \cdot \mathbf{J}_b &= \mathbf{E}_{in} \cdot (\mathbf{J}_f + \mathbf{J}_d - \mathbf{J}_b) \\ &= \mathbf{E}_{in} \cdot \mathbf{J}_f + \mathbf{E}_{in} \cdot \mathbf{J}_{int} \ , \end{aligned} \tag{4}$$

where we have defined $\mathbf{J}^{int} = \mathbf{J}_d - \mathbf{J}_b$.

From (1)-(3) we obtain the uncoupled integral equations

$$\mathbf{E}_{in}(\mathbf{r}) = \frac{\mathbf{J}_b(\mathbf{r})}{\sigma_b(\mathbf{r}) - \sigma_h} - \mathbf{E}(\mathbf{r})\,[\mathbf{J}_b] \tag{5}$$

$$\mathbf{E}_{in}(\mathbf{r}) = \frac{\mathbf{J}_f(\mathbf{r})}{\sigma(\mathbf{r}) - \sigma_b(\mathbf{r})} - \mathbf{E}(\mathbf{r})\,[\mathbf{J}_f] \tag{6}$$

$$\mathbf{E}_{ef}(\mathbf{r}) = \frac{\mathbf{J}^{int}(\mathbf{r})}{\sigma(\mathbf{r}) - \sigma_h} - \mathbf{E}(\mathbf{r})\left[\mathbf{J}^{int}\right] \ , \tag{7}$$

where the effective incident field, $\mathbf{E}_{ef}(\mathbf{r})$, is given by

$$\mathbf{E}_{ef}(\mathbf{r}) = \frac{\sigma_b(\mathbf{r}) - \sigma_h}{\sigma(\mathbf{r}) - \sigma_h}\mathbf{E}\,[\mathbf{J}_f] + \frac{\sigma(\mathbf{r}) - \sigma_b(\mathbf{r})}{\sigma(\mathbf{r}) - \sigma_h}\mathbf{E}\,[\mathbf{J}_b] \ . \tag{8}$$

The algorithm for eliminating the background is:

1. Solve (5) for $\mathbf{J}_b$ using a coarse background grid, G_b
2. Solve (6) for $\mathbf{J}_f$ using a fine grid, G_f, covering only the flaw
3. Solve (7) for $\mathbf{J}^{int}$

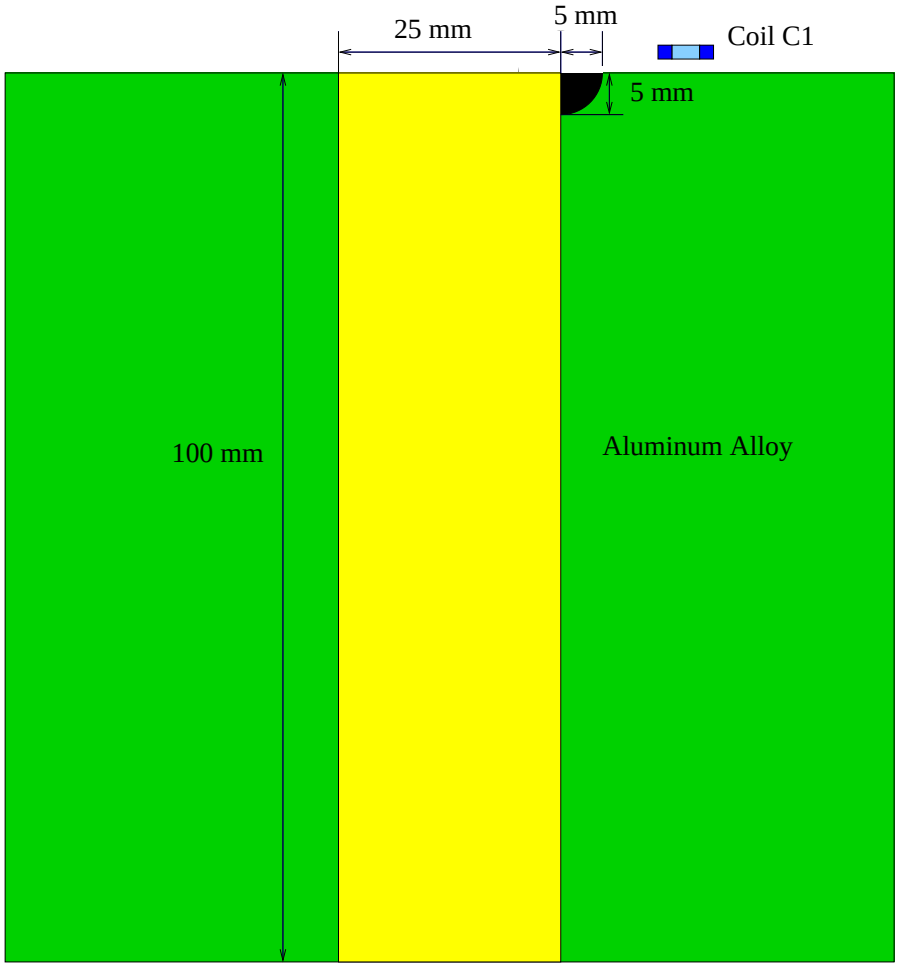

FIGURE 2. Benchmark Problem 1: Notch in a bolt hole through an aluminum block. The coil for the test, C1, is shown roughly to scale.

and then compute the change in the probe impedance, due to the flaw, as

$$\Delta Z_{\text{flaw}} = \mathbf{E}_{in} \cdot \mathbf{J}_f + \mathbf{E}_{in} \cdot \mathbf{J}^{int(b)} + \mathbf{E}_{in} \cdot \mathbf{J}^{int(f)} \tag{9}$$

where the dot products are the usual expressions for impedances [1]. An attractive feature of this system is that the flaw and background may be gridded separately, in a manner appropriate to their size and characteristic.

NOTCH AT A BOLT HOLE BENCHMARK PROBLEMS

Benchmark Problem 1 is shown in Figure 2, and Benchmark Problem 2 is shown in Figure 3. The two coils that are used in the benchmark problems are described in Table 1. C1 will be used to collect data for benchmark1 and H1 for benchmark2. The values of C_p, L_0, and R_0 are determined by fitting the measured data of the coils in air with the usual circuit model of a one-port probe, which consists of a parasitic admittance element, Y_p, in shunt with a series impedance $R_0 + j\omega L_0$.

MODEL-BASED INVERSION WITH NLSE

After removing the shunt parasitic admittance element, Y_p (which includes the capacitance, C_p), of each coil, and then removing the freespace impedance, $R_0 + j\omega L_0$,

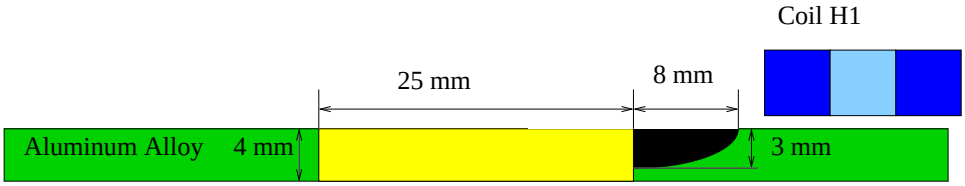

FIGURE 3. Benchmark Problem 2: Notch in a bolt hole through a 4mm thick aluminum plate. The coil for the test, H1, is shown roughly to scale.

TABLE 1. Data for Coils C1 and H1: Dimensions in mm.

Coil	ORadius	IRadius	Height	No. Turns	C_p(pF)	L_0(H)	$R_0(\Omega)$
C1	4	1.58	1.042	305	13.85	463×10^{-6}	19.08
H1	7.38	2.51	4.99	4000	72.8	0.10052	688.4

we are left with the 'air-balanced' change in impedance, δZ, when the coil is placed over the workpiece. This is the input to NLSE for inverting each of the datasets known as M1, M2, M3, and M4 for each of the two benchmark tests. (The datasets correspond to four different locations on the unflawed workpiece.) The purpose of the inversions is to determine the host conductivity and coil liftoff for each of the benchmark tests. Even though each dataset contained values of δZ at 32 frequencies logarithmically spaced between 500Hz and 500KHz, we used only five frequencies for the inversions. For benchmark 1, we used the five highest frequencies, 205.06kHz, 256.24kHz, 320.2kHz, 400.13kHz, and 500.0kHz, and for benchmark 2 the five lowest frequencies, 500Hz, 624.8Hz, 780.76Hz, 975.65Hz, and 1219.2Hz. The reason for this separation is due to the fact that the coil for benchmark 1, C1, has a very small inductance, as is seen from Table 1, whereas that for H1 is quite large. Therefore, we get more reliable data at high frequencies for C1 and at low frequencies for H1. The inversion results are shown in Table 2 for benchmark 1, and in Table 3 for benchmark 2.

When we use the coil data of Table 1 and the results of data set M1 of benchmark 1 in Table 2 to compute the forward model, and then plot the results over the entire frequency range of 500Hz to 500kHz, we obtain Figure 4. (The data are normalized with respect to frequency.) That there is a breakdown in the measured resistance data at low frequencies (dR goes negative!) was anticipated because of the considerable uncertainty of Y_p for coil C1 at low frequencies. The corresponding results for M1 of benchmark 2 in Table 3 are shown in Figure 5. The results for the other data sets in Tables 2 and 3 lie on top of the results shown in Figures 4 and 5. The high-frequency breakdown in the resistance and reactance in Figure 5 was anticipated because of the uncertainty in Y_p for H1 at high frequencies. Note, however, that the normalized model reactance, dX/f, due to NLSE in Figure 5 'saturates' at high frequencies, as expected by classical coupled-circuit theory and Förster plots. The asymptote is a measure of the coupling of the coil to the host. The asymptotic value of $dR/f = 0$ is reached at a higher frequency in Figure 5, as is also predicted by coupled-circuit theory.

TABLE 2. NLSE inversion results for benchmark 1 datasets.

Data Set	Φ	σ(S/m)/sensitivity	LO(mm)/sensitivity
M1	4.9166	1.8156(7)/2.73(-2)	0.1336/1.262(-2)
M2	4.8827	1.8151(7)/2.74(-2)	0.1364/1.255(-2)
M3	4.6704	1.8178(7)/2.63(-2)	0.1420/1.205(-2)
M4	4.8004	1.8175(7)/2.69(-2)	0.1389/1.236(-2)

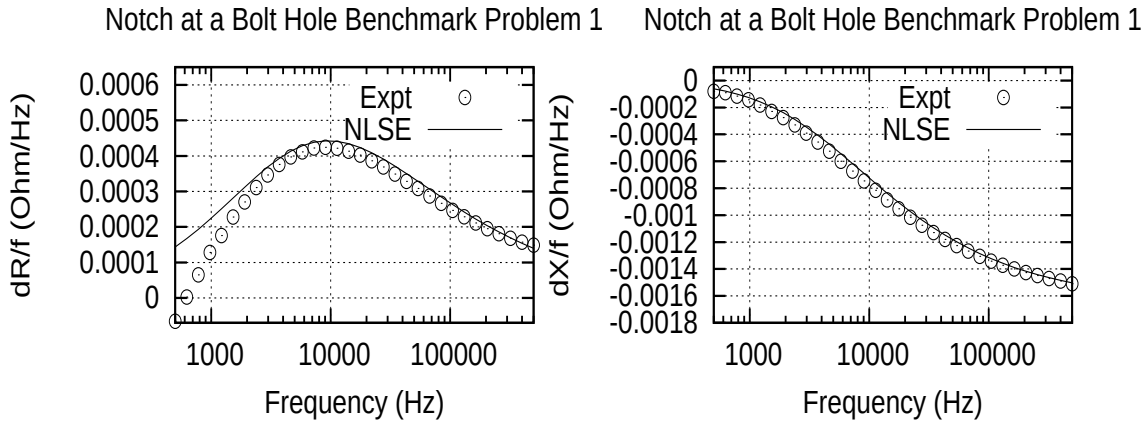

FIGURE 4. Comparing the normalized model results and data sets for M1 of benchmark 1 in Table 2 over the entire frequency range.

TABLE 3. NLSE inversion results for benchmark 2 datasets.

Data Set	Φ	σ(S/m)/sensitivity	LO(mm)/sensitivity
M1	0.6385	1.8340(7)/4.03(-3)	0.3480/1.542(-2)
M2	0.8585	1.8420(7)/5.46(-3)	0.3560/2.075(-2)
M3	0.7850	1.8390(7)/4.97(-3)	0.3550/1.899(-2)
M4	0.3887	1.8227(7)/2.41(-3)	0.3254/0.933(-2)

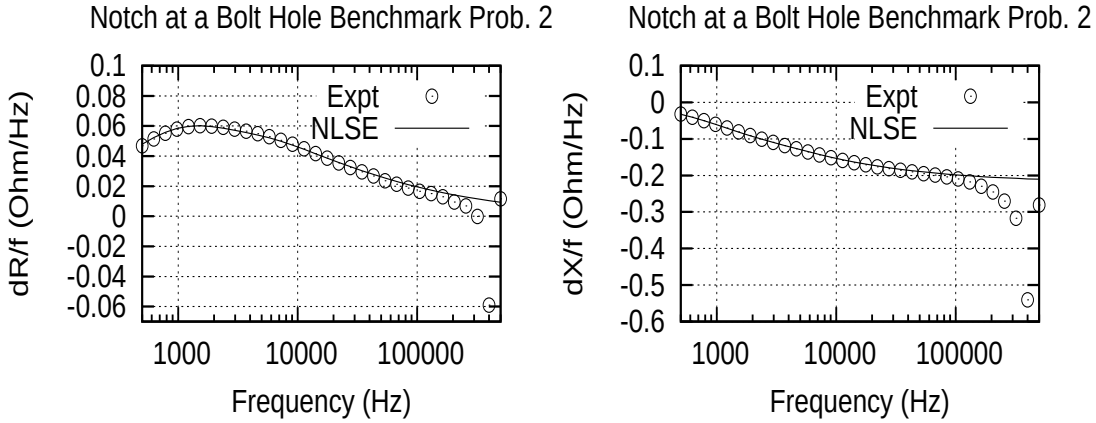

FIGURE 5. Comparing the normalized model results and data sets for M1 of benchmark 2 in Table 3 over the entire frequency range.

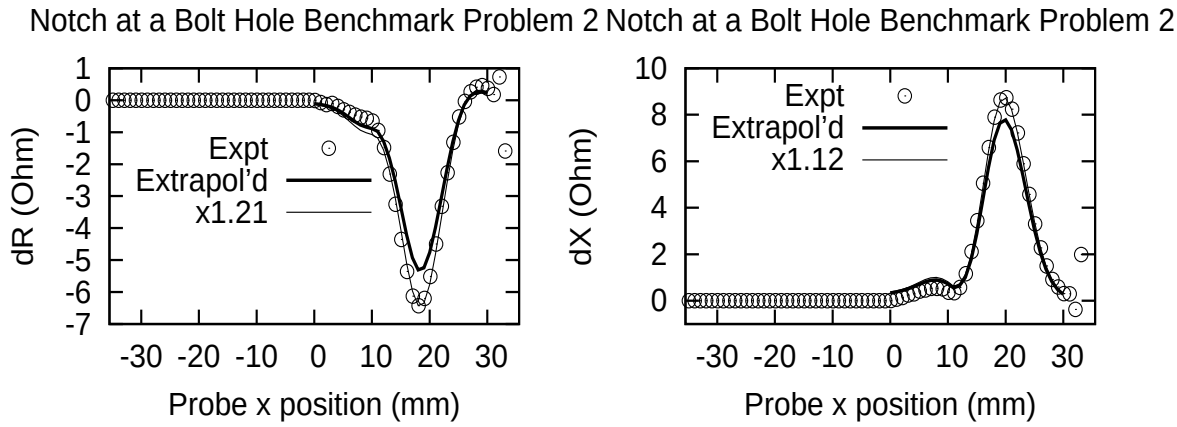

FIGURE 6. Comparison of measured values of the change in impedance to values computed using different grids for the bolt hole in Benchmark Problem 2. The scan is along $Y = 0$.

FINAL RESULTS OF THE BENCHMARK TESTS

The final results of our validation studies for the multi-scale algorithm are plotted in Figure 6 for Benchmark Problem 2 and Figure 7 for Benchmark Problem 1. Numerical experiments show that accurate results for Benchmark Problem 2 require a background grid that is much finer near the notch. We can obtain results that effectively use a graduated grid which becomes progressively finer in regions closer to the notch. It is clear, however, from varying the number of notch cells that the impedances we are trying to compute have not converged with respect to number of cells along the x, y, or z directions for a grid of 32 x 2 x 16 cells.

It is also clear from varying the number of background (bolt-hole) cells that the impedances have not converged with respect to number of cells along the x, y, or z directions for a grid of 16 x 16 x 4 cells.

We can improve our impedance values by combining them with values obtained from an 8 x 8 x 2 cell graduated grid for the bolt hole and a 16 x 2 x 8 cell notch grid. This allows us to perform a linear extrapolation to zero cell dimensions. That is the result labeled 'Extrapol'd' in Figure 6.

As with Benchmark Problem 2, accurate results for Benchmark Problem 1 require a background grid that is much finer near the notch, and so we again apply the graduated-grid scheme that was used for that problem. We also use the extrapolation procedure that was used in Problem 2, with the result labeled 'Extrapol'd' in Figure 7.

The response of the small notch is clearly evident in both benchmark problems, and its shape agrees with the measured data, which were the goals of the algorithm, but the absolute values differ by 12% to 39%, with the smaller errors occuring in Benchmark Problem 2. The reason for the discrepancies in scale is due to the size of the problems. Benchmark Problem 1 contains a hole that is abnormally large compared to the notch, and at the excitation frequency of 5kHz, this hole requires a huge number of cells. Benchmark Problem 2 is somewhat more realistic in its size, and the extrapolated results are closer in scale to the measured data. We have ideas for improving the convergence of the algorithm for large problems, and they will be explored in future

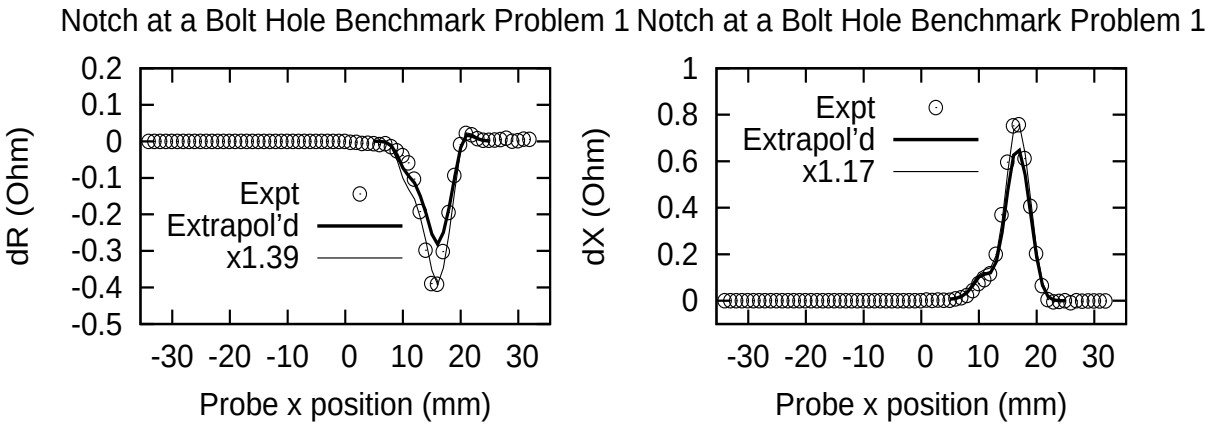

FIGURE 7. Comparison of measured values of the change in impedance to values computed using different grids for the bolt hole in Benchmark Problem 1. The scan is along $Y = 0$.

research.

ACKNOWLEDGEMENTS

This work was supported by the Air Force Research Laboratory through contract FA8650-09-C-5232 with Victor Technologies LLC.

REFERENCES

1. H. A. Sabbagh, R. K. Murphy, E. H. Sabbagh, J. C. Aldrin, J. S. Knopp, and M. P. Blodgett, 'The Joy of Computing with Volume Integrals: Foundations for Nondestructive Evaluation of Planar Layered Media,' ACES Journal, Vol. 25, No. 9, Spetember 2010, pp. 723-730.